Compact Platform Tolerant UHF RFID Tag for Near Field RF Applications

Abhishek Choudhary, Deepak Sood, and Krishan Gopal
Electronics and Communication Department, University Institute of Engineering and Technology, Kurukshetra University, Kurukshetra (136119), Haryana, India

Corresponding author: Abhishek Choudhary (e-mail: choudhary.abhi16@gmail.com).

ABSTRACT A T-matched meander line passive platform-tolerant Radio Frequency Identification (RFID) tag is designed for near-field Ultra High Frequency (UHF) communication. A new method is introduced to effectively limit the read range of the UHF RFID tag, ensuring its functionality within the near-field region. The proposed compact RFID tag antenna, with overall dimensions of 43 x 10 x 1.6 mm³, demonstrates strong electric and magnetic fields in the near-field region. The tag incorporates the Higgs 4 IC chip from Alien Technology, which provides enhanced sensitivity and a rapid read rate for storing unique identifiers. Comprehensive read range measurements were conducted on various common mountable platforms. Key performance metrics, including impedance, radiation pattern, bandwidth, and the impact of ground size on gain, were thoroughly analyzed. Experimental results confirm that the proposed tag exhibits robust identification capabilities in the near-field zone, making it well-suited for item-level tagging applications.

INDEX TERMS RFID Tag, UHF, Near Field Communication, Platform tolerant.

I. INTRODUCTION

RADIO Frequency Identification (RFID) technology has experienced rapid growth over the past decade, utilizing radio frequency signals for the automatic identification of objects. RFID is employed across a diverse range of sectors, including agriculture, healthcare, aviation, libraries, military, passport control, supply chain management, inventory tracking, the aircraft industry, mobile payment systems, and smart parking applications. Communication between RFID readers and tags operates differently depending on the operational frequency bands. In the low-frequency (LF) band (125-134 kHz) and high-frequency (HF) band (13.56 MHz), interactions are facilitated through magnetic (inductive) near-field coupling, resulting in a detection range limited to several tens of centimeters. Conversely, ultra-high frequency (UHF) band (860-960 MHz) and microwave band (2.4 GHz and 5.8 GHz) RFID systems enable long-range communication through electromagnetic wave propagation between reader and tag antennas [1]. UHF RFID passive tags, designed for near-field communication (NFC), generally offer better transmission rates, data storage, and exchange capabilities compared to LF and HF tags due to their higher frequency and wider bandwidth. UHF RFID tags ensure reliable performance in close-range communication, even in environments with interference. While certain HF tags may offer larger memory sizes, UHF tags remain the better choice for supporting fast and reliable data exchange in near-field communication and can support item-level tagging. Consequently, UHF RFID technology is widely regarded as the preferred and established standard for major applications [2]. To leverage the benefits of the UHF band for near-field RFID applications, such as item-level tagging (ILT) [3], electronic payment, ID cards, and e-passports [4], it is essential to confine the detection range within the desired interrogation volume. The induced voltage at the antenna terminals is proportional to the operating frequency [5]. Consequently, transitioning from the HF to the UHF band represents a significant advantage in terms of energy transfer between RFID devices. As the available power transferred increases, the system's ability to overcome environmental impairments also improves. While the UHF RFID system offers extended range capabilities, it often results in unintentional detection of multiple tags. Moreover, in applications such as retail environments, warehouses, libraries, manufacturing plants, and airports, the reliability of item-level tagging (ILT) is compromised due to interference among multiple tags and readers. Consequently, the desired product can be identified through filters in the UHF interface or algorithms within the middleware [6]. This additional processing increases both programming and integration efforts, thereby raising the overall costs of UHF systems. Therefore, a UHF RFID system designed to operate within the near-field region could provide a more effective solution.

Short-range detection in the UHF band can be achieved by designing special reader antennas specifically for near-field communication using techniques such as inductive coupling [3], [7-10], in which single or multiple loops are created to expand the interrogation zone in the near-field region of the reader antenna. The design reported in [3] employed a

quadruple-loop antenna, while in [7], a dual-printed-dipole structure was designed to realize an electrically large loop with in-phase current. Furthermore, in [8], a folded square-loop antenna design is reported that provides a uniform magnetic field in the zone near the antenna. The design discussed in [9] incorporated a closely spaced, two-element Zero-Phase-Shift-Line (ZPSL) loop array. The design reported in [10] employed multiple rectangular loops, each formed by incorporating two semi-loops, with one printed on the top side of the dielectric substrate and the other on the bottom side. As a result, the magnetic field is reinforced inside the loop, which is defined as the interrogation zone of the antenna. Another approach to achieve near-field RFID communication is electrical coupling, as discussed in [11-12]. In this case, the reader antenna consists of rectangular/circular slots in the ground, fed by microstrip lines that are left open-circuited. The electric fields are created inside the slots for RFID tag coupling. All pairs of slots are spaced $\lambda_g/2$ apart, since the distance between successive current maxima is $\lambda_g/2$. Leaky microstrip lines [13-15] are another technique that enables tag detection in a selectively confined region. In all the aforementioned reader antenna design techniques for near field communication in the UHF band, the size of the antenna is very large, as multiple loops, slots, or long strips are required to provide a sufficient interrogation zone for tag detection. Furthermore, the detection range of conventional reader antenna can be confined by using a metamaterial grid formed by an array of metallic strips that helps [16-19] to block the radiation field in the direction of the tag. This makes the arrangement complex and large in size. Another technique to limit the read range is to design the UHF RFID tag itself for the near field region, to serve applications like item level tagging, temperature sensing [20], in biomedical systems where tags are implanted inside the body to collect electromyography (EMG) [21] and electroencephalogram (EEG) [22] signals, intracranial pressure [23]. Additionally, the nearfield tags can be integrated into radiofrequency finger-augmentation devices (RFAD) [24-25]. The various configurations to design the UHF RFID tag for near field range includes meandering [2] , use of loop and coil type configurations [26] for forming the unidirectional current to establish uniform magnetic field and use of complementary split ring structures [27]. Meandered loops [28], the combination of loop and meandering/ logarithmic spiral are used, to establish inductive coupling [29]. Further, T-matching [30] is used to control the impedance of the tag. Other challenges to design UHF RFID tag for near field applications include optimizing the impedance matching of tag antenna with chip [31], use of low-dielectric loss materials [1] to minimize signal attenuation and implementing design features that reduce sensitivity to orientation and alignment issues thereby helping to avoid unwanted reads from powerful far-field readers [31]. The novelty of this work lies in the development of a unique technique to confine the read range of a near-field UHF RFID tag by reducing the radiation resistance of the tag antenna. Various approaches are reported to reduce radiation resistance of tag antenna such as optimizing the size of ground plane [32], adjusting substrate thickness, and using high dielectric constant [33] material as substrate. A reduction in radiation resistance leads to a decrease in the antenna's radiation efficiency and gain, effectively limiting its read range to the near-field region. In the presented design, a metallic ground plane is incorporated on the backside of the tag's mounted substrate to achieve reduction in the radiation resistance of the tag through image current cancellation effect [34]. Furthermore, the size of the tag is optimized by incorporating meandering to ensure best fit impedance matching for maximum energy transfer from the tag antenna to the chip. This strategic use of the ground plane not only enhances the compactness of the tag but also contributes to make the design platform-tolerant, thereby increasing its adaptability for a variety of mounting configurations. Experimental validation of these design elements confirms the effectiveness of this approach for item-level tagging applications, offering improved control over the read range and overall tag performance.

The paper is organized as follows. Section II presents the design, optimization, and analysis of the proposed near-field UHF RFID tag. This section covers the detailed design process, simulation results, field distribution, and radiation pattern analysis. Section III focuses on the experimental evaluation, where the impedance, return loss (S_{11}), read range, read rate, and path gain of the tag are measured and analyzed across various mounting surfaces. Finally, Section IV summarizes the key findings and presents the conclusions of the study.

II. DESIGN & ANALYSIS

An EPC global class 1 Gen 2 Higgs 4 IC chip manufacturing by Alien Technology [35] is used to design the proposed tag. The equivalent circuit model of IC chip consisting a resistor of 1.8 KΩ connected in parallel with a small valued capacitor of 0.95 pF is shown in Fig. 1. The impedance of the chip at 866 MHz can be calculated using "(1)".

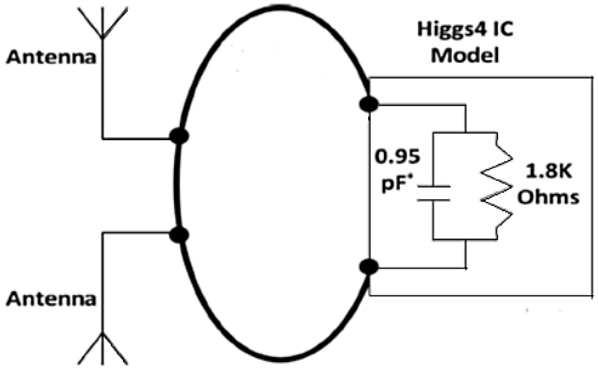

FIGURE 1. Circuit model of the RFID IC impedance.

$$Z_{IC} = R \parallel X_C \quad (1)$$

$$X_C = \frac{-j}{2\pi f_r C} = \frac{-j}{2\pi \times 866 \times 1.8 \times 10^6 \times 0.95 \times 10^{-12}} = -j193.45$$

$$Z_{IC} = (1.8\ K\Omega) \parallel (-j193.45)$$

$$= 20.55 - j\ 191.45\ \Omega$$

The tag is designed and optimized using the HFSS (High Frequency Structure Simulator). In the first phase of tag design process for near field applications, a metallic loop antenna is designed with an objective to achieve strong uniform magnetic field coupling. The loop antenna is patterned on an ungrounded substrate FR4 (ε_r = 4.4 and tan δ = 0.02) of thickness 1.6mm. The dimensions of the loop is optimized with an aim to match its impedance with that of UHF RFID chip. The optimized dimensions of the loop antenna are L = 22.21 mm, 'W' = 6 mm and trace width is 1mm as shown in Fig. 2 (a). The loop antenna is made up of copper of thickness 35 µm. The impedance of the optimized loop is 0.91 + 191.52j Ω at 866MHz as shown in Fig. 3. With the best efforts it is observed that only imaginary part of the loop is matched with the chip. For the optimized loop dimensions the radiation efficiency and gain are obtained as 10.45% and -8.24 dBi respectively. The reading range of this loop antenna is calculated using Friss transmission equation with the transmitting power of the reader as 2W EIRP. The calculated range of this loop antenna is 2.03 m. Further, in order to obtain the best fit of the design, the matching of real part of the proposed design with that of the chip is done, by incorporating meandering [36] on both sides of the loop as shown in Fig. 2(b). The optimized dimensions of this design are given in Table I.

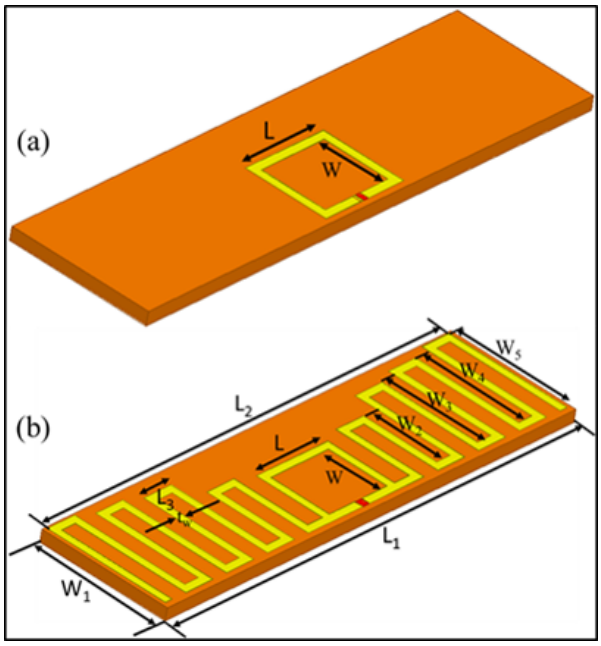

FIGURE 2. Geometry of the ground less (a) loop tag antenna (b) loop tag antenna with meandering.

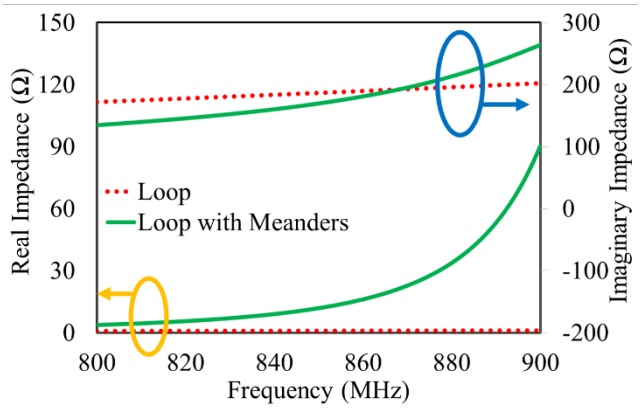

FIGURE 3. The simulated impedance of the ground less loop and loop with meandering.

The impedance of the optimized loop with meandering is 19.73 + 189.1j Ω at 866MHz as shown in Fig. 3. The radiation efficiency and gain of 83.28% and 1.34 dBi respectively. The calculated range of this antenna is 15.18 m. It is observed that use of meandering not only increases the efficiency and gain but the range as well, which makes this tag antenna suitable for far field UHF applications.

TABLE I. Dimensions of ground less loop tag antenna with meandering.

Parameters	Dimensions (mm)	Parameters	Dimensions (mm)
L	10.5	W_1	17
L_1	60	W_2	10
L_2	59	W_3	13
L_3	4	W_4	14
W	8	W_5	16
t_w	1	H	1.6

In the next phase of the design process a technique is adopted to confine the range of the designed UHF RFID tag. In order to confine the read range, a ground plane is embedded to the designed tag as represented in Fig.4. The purpose of adding the ground plane with the antenna is to achieve the two objectives. One is to make the tag be tolerant for different mountable surfaces and the second one is to reduce the radiation efficiency through image current cancellation effect so that its working range be confined to near field region [34]. The dimensions are re-optimized after the incorporation of ground plane as listed in Table II.

TABLE II. Dimensions of ground less loop tag antenna with meandering.

Parameters	Dimensions (mm)	Parameters	Dimensions (mm)
L	8.9	W	6
L_1	43	W_1	10
L_2	42	W_2	3
L_3	3	W_3	4
t_W	1	W_4	4
H	1.6	W_5	9

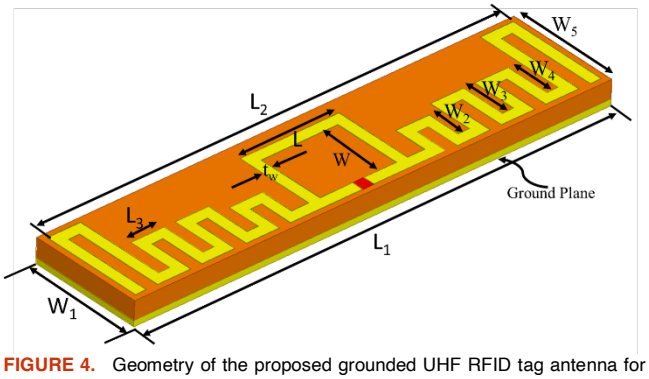

FIGURE 4. Geometry of the proposed grounded UHF RFID tag antenna for near field operation.

In order to achieve the final optimized configuration of the tag antenna the design process is initiated with the design of T-match loop along with straight microstrip dipole antenna as shown in Fig. 5(a). The T-matched loop provides an inductive effect, while the straight dipole provides a resistive effect in the impedance of the overall antenna. However, incorporating the straight dipole causes the antenna size to become very large. Therefore, in the next step, shown in Fig. 5(b), '1×2' meanders are incorporated into the dipole. This reduces the length of the antenna to 62.1 mm, while keeping the resonance frequency of the antenna fixed at 866 MHz. Further, by incorporating '2×2' meanders as shown in Fig. 5(c), the antenna size reduces to 47.8 mm, and the use of '3×2' meanders, shown in Fig. 5(d), reduces the length to 42.5 mm. The lengths of the meanders can be varied individually to control the resonance of the antenna for the required frequency. Finally, by incorporating '4×2' meanders as shown in Fig. 5(e), the antenna length reduces to 42 mm

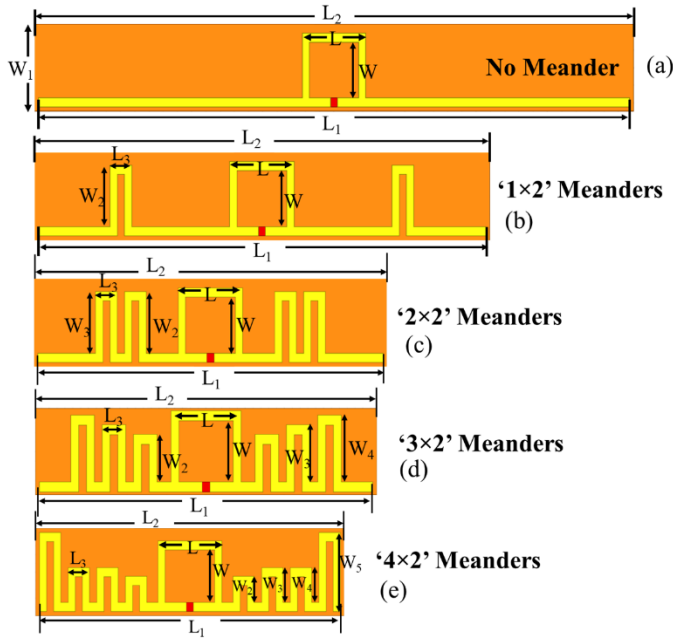

FIGURE 5. The evolution of the design of the Near Field UHF band T-matched meanderline tag antenna. (a) T-match loop with straight dipole. (b) T-matched loop with '1×2' meandered dipole. (c) T-match loop with '2×2' meandered dipole. (d) T-match loop with '3×2' meandered dipole. (e) T-match loop with '4×2' meandered dipole.

while maintaining the same resonance frequency of 866 MHz. The dimensions of the tag antenna for different configurations in the design process are listed in Table III. The impedance and return loss (S_{11}) responses for all the configurations are shown in Figs. 6(a) and 6(b). It is clear from the responses that the resonance frequency of the antenna can be maintained while reducing its size (or increasing the number of meanders). The lengths of the meanders in the design increase from the port to the outer side of the antenna. The inner meanders are shorter compared to the outer meanders, as the current magnitude in the middle portion of the dipole is higher and decreases as it moves away from the center towards the outer portion thereby, the middle meanders lead to more losses than the meanders located at the outer edges of the antenna [37]. Therefore, it is preferable to use longer meanders at the outer edges of the tag antenna and shorter meanders near the middle portion. Hence, meandering configurations can be used as a parameter for controlling the radiation efficiency of the meanderline antenna.

TABLE III. Dimensions of ground less loop tag antenna with meandering.

Meanders	L	L_1	L_2	L_3	W	W_2	W_3	W_4	W_5
No	8.9	83.1	84.1	-	7.4	-	-	-	-
1×2	8.9	62.1	63.1	3	7.4	6.7	-	-	-
2×2	8.9	47.8	48.8	3	7.4	6.7	6.7	-	-
3×2	8.9	42.5	43.5	3	7.4	4.96	5.96	6.96	-
4×2	8.9	42	43	3	7	3	4	4	9

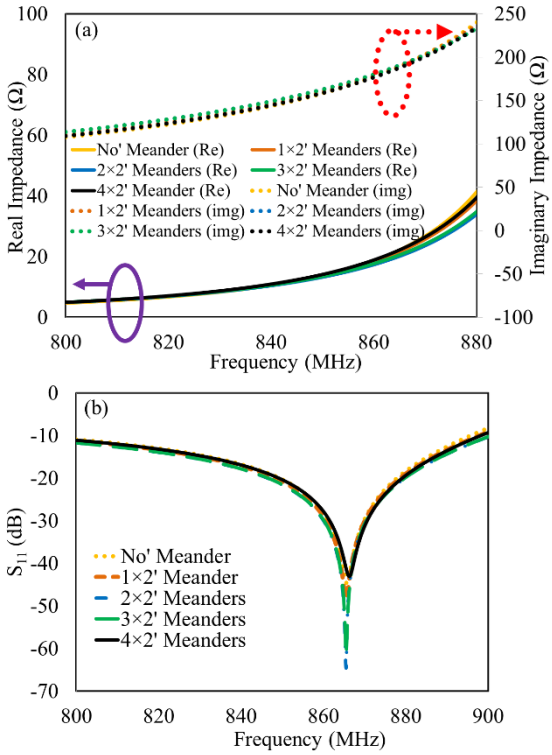

FIGURE 6. **(a)** The real and imaginary impedance of the design with all the configurations. (b) Return losses (S_{11}) in dB of the design with all configurations.

The resistance and inductance of the antenna increase with the increase in the length of the meander as shown in Fig. 7(a) and 7(b). Optimized dimensions of the meanders are 'W_2 = 4mm', 'W_3 = 5mm', 'W_4 = 5mm', and 'W_5 = 9mm'.

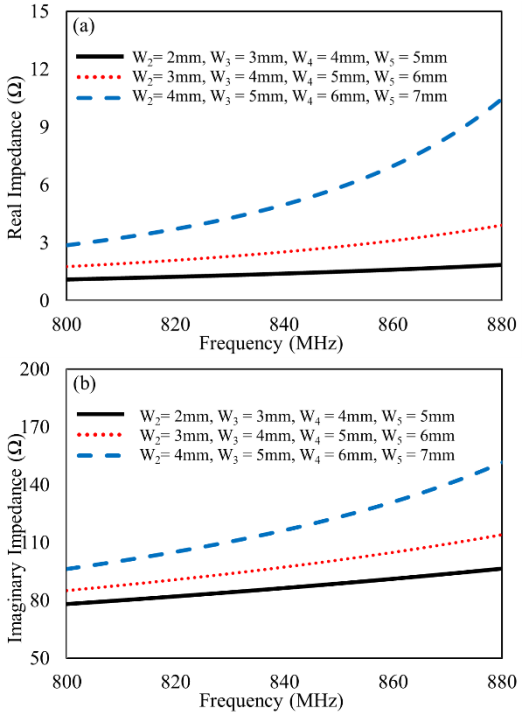

FIGURE 7. Variation in the impedance of the antenna by changing the length (W_2, W_3, W_4, and W_5) of the meanders, (a) Real impedance (b) Imaginary impedance.

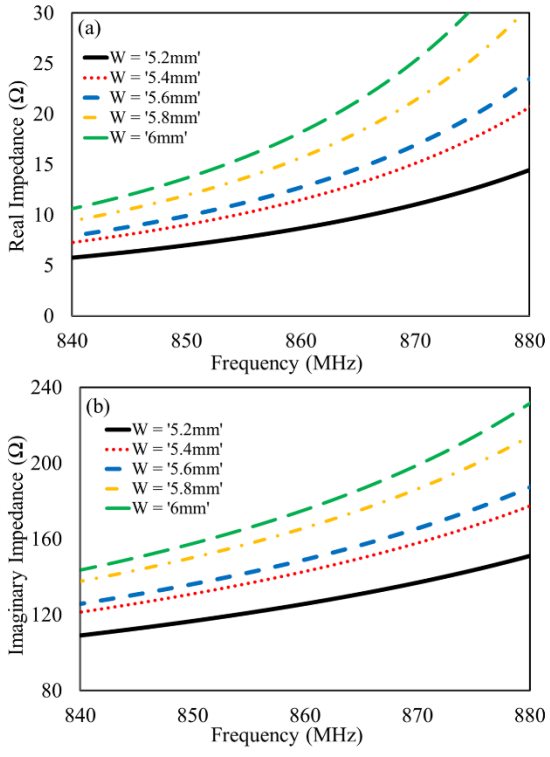

FIGURE 8. Variation in the impedance of the antenna by changing the loop side (W) of the Loop, (a) Real impedance (b) Imaginary impedance.

The impedance of the antenna can also be controlled by T-match loop's side 'W' as shown in Fig. 8(a) and (b). The resistance and inductance increase with the increase in the loop's side 'W' of the antenna. Therefore, the optimized dimension of the 'W' is 6 mm. To gain more physical insight of the design for its near field operation, the current and field distributions of the tag antenna are studied as shown in Fig. 9. Since the overall size of the tag is much less than the operating wavelength thereby the surface current at 866 MHz is unidirectional in the tag antennas shown in Fig. 9 (a), which helps to establish uniform field distribution. It is observed that the magnetic field in Fig. 9 (b) is more concentrated near the loop of the design and the electric field Fig. 9 (c) is highly distributed at the edges of the tag. This indicates the strong field coupling capability of the tag with the any conventional reader antenna.

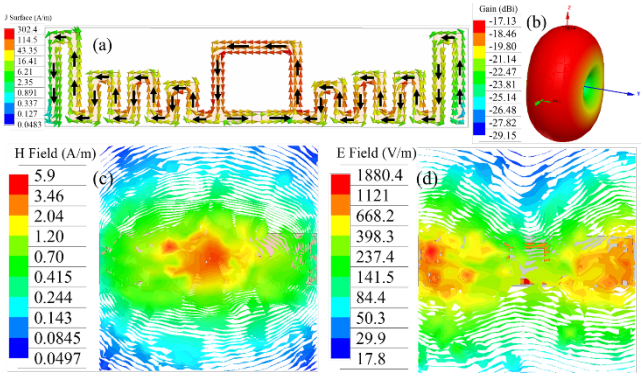

FIGURE 9. (a) Current distribution (b) radiation pattern (c) magnetic field distribution and (d) electric field distribution at 5mm above the grounded tag.

Moreover, the electric field is due to horizontal portion of the meanders 'L_3', as the current in the two adjacent vertical components is out of phase due to which the field generated by these vertical components cancel out each other. Hence, the incorporation of a ground plane reduces the radiation efficiency to 1.2%, resulting in a very low gain of -17.13 dBi, as shown in the omnidirectional radiation pattern in Fig. 9(d). The reduced efficiency and gain help to confine the range of the UHF RFID tag. Further, the impedance of the designed tag is analyzed with and without using the ground plane. In groundless configuration, the resonant frequency of the tag antenna is changes due to the variation in the impedance of the tag antenna as shown in Fig. 10 (a) and (b). The impedance is controlled intentionally to confine the range of RFID tag in near field region. Fig.11 shows the radiation pattern with and without ground plane. In groundless configuration, the antenna gain improves due to the increase in the radiation efficiency (21.22%) of the antenna. This compensates for the loss caused due to impedance mismatching. The design is also analyzed for different sizes of metallic ground plane. It is observed that the impedance of the antenna remains unaffected as long as the size of the ground is equal to or

greater than the size of the substrate. However, if the size of the ground is smaller than the size of the tag antenna, then the impedance of the antenna changes due to the reduction in the inductance and resistance created by the image component of the top meandered dipole under the ground plane as shown in Fig. 12.

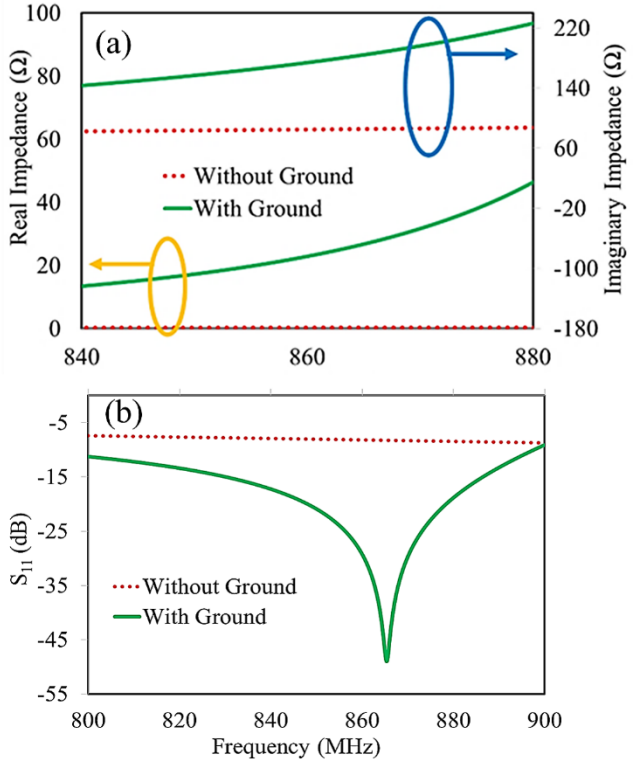

FIGURE 10 (a) Impedance and (b) return loss variations of the tag for grounded and ground-less configurations.

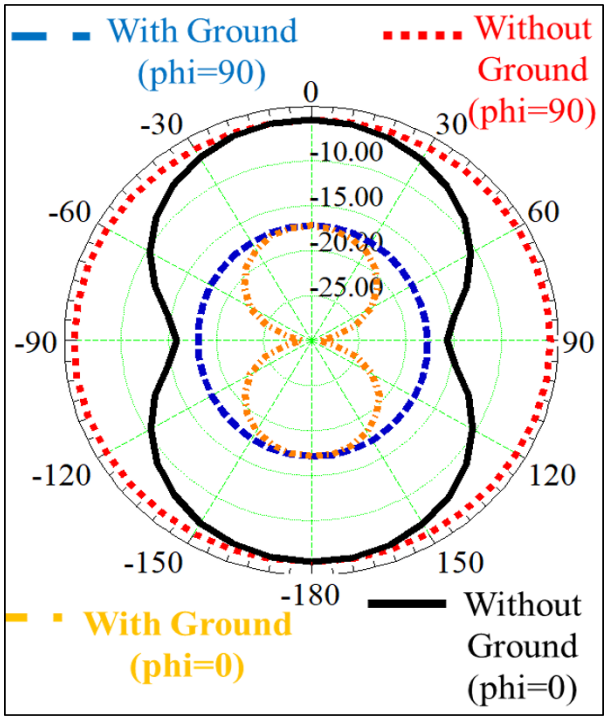

FIGURE 11. Radiation pattern of the designed tag for grounded and ground-less configurations.

The variation in the ground plane also affect the radiation efficiency and gain of the antenna as shown in Fig. 13.

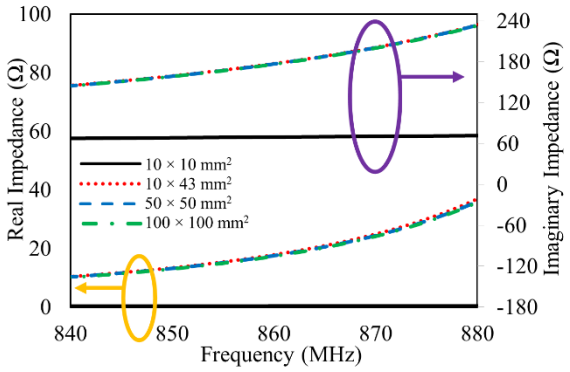

FIGURE 12. Impedance study for the variation of the ground plane size.

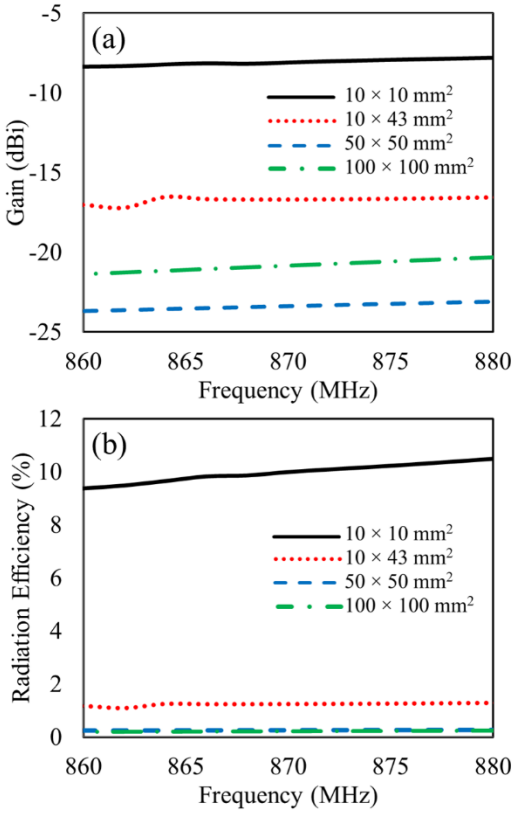

FIGURE 13. Effect of the variation of the ground plane size on the (a) radiation efficiency and (b) gain of the antenna.

. It is observed that the radiation efficiency decreases significantly with the increase in the size of the ground as shown in Fig. 13(a), but the corresponding gain increases as the size of the ground increase from 10 × 10 mm^2 to 100 × 100 mm^2 as depicted in Fig. 13(b) There is a reduction in the back lobe by increasing the size of the ground and which consequently increases the directivity of the antenna. When the size of the ground is reduced as compared to the size of the antenna, the radiation efficiency as well as the gain of the

antenna increases, due to the failure of image effect under the ground plane.

III. MEASUREMENTS

The fabricated prototype of the tag is shown in Fig. 14. The top patch (Fig. 14 (a)) and bottom ground layer (Fig. 14 (b)) are fabricated using copper of thickness 35 µm and the substrate used is epoxy FR4 of thickness (h) = 1.6 mm, dielectric constant of $\varepsilon_r = 4.4$, and a loss tangent (tan δ) = 0.02. The size of the fabricated tag is (43 × 10 × 1.6) mm^3.

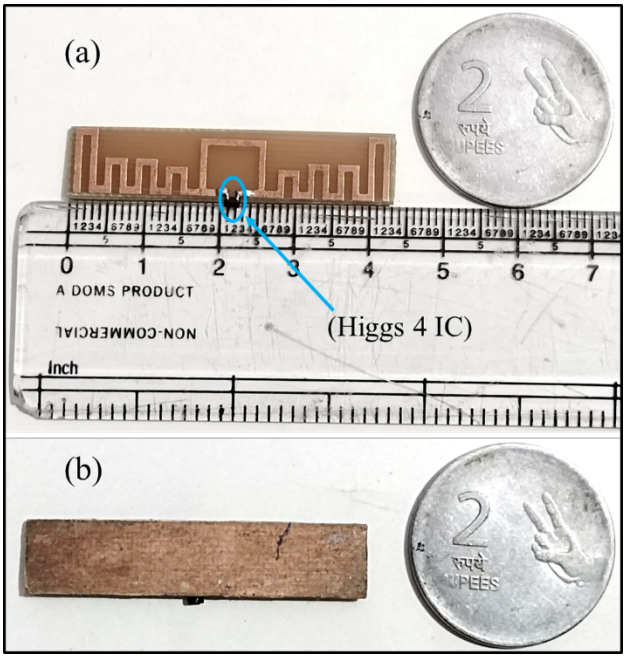

FIGURE 14. Prototype of the proposed tag. (a) Top view, (b) Bottom view.

The impedance of the UHF RFID near field tag is measured using (VNA) of the PNA series model N5222A as shown in Fig. 15. The test fixture (differential probes) is constructed by using two rigid RG 405 coaxial cables with an outer conductor diameter of 2.18 mm. The outer conductors of the coaxial cables are soldered together along the length. One end of the fixture is soldered with two subminiature version A (SMA) female connectors and the other end of the fixture is kept open with the small extensions of inner conductors to form the tips to connect the tag antenna under test. The SMA female connectors in the fixture are connected to the VNA through test cables. The VNA is calibrated and the calibration plane is extended to the end of the test probe after port extension. In order to reduce calibration error the probe lengths are taken as equal. The tag antenna is connected to the end tips of the fixture and S parameters are measured and the differential impedance is calculated [38] by putting these S parameters in equation (2).

$$Z_d = \frac{2Z_0(1-S_{11}^2+S_{21}^2-2S_{12})}{(1-S_{11})^2-S_{21}^2} \quad (2)$$

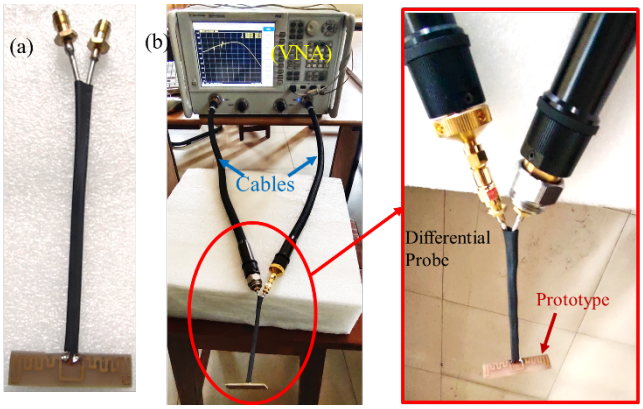

FIGURE 15. Measurement setup. (a) Fixture Prototype (b) Measurement setup using vector network analyzer.

Here, Z_0 is the characteristic impedance (50 Ω) of the coaxial cable used in differential probe. S_{11}, S_{21}, and S_{12} are the scattering parameters. The measurements are done by placing the prototype on different materials like free space, metal and skin etc. The simulation of the tag design is also done on the human arm. A human arm was modelled by four tissues layers (skin, fat, muscle and cortical bone) as shown in Fig. 16. The thickness and frequency-dependent permittivity (ε_r), and conductivity (σ) [39] are shown in Table IV.

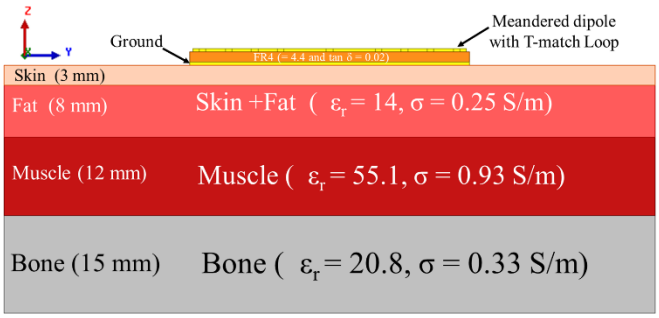

FIGURE 16. A model of the Human arm with four tissues layers (skin, fat, muscle and cortical bone).

TABLE IV. Thickness and dielectric electric property of the different tissue's layers in the arm model.

Layers	ε_r	σ (S/m)	Thickness (mm)
Skin + Fat	14	0.25	3 (Skin) + 12 (Fat)
Muscle	55.1	0.93	10
Bone	20.8	0.33	3

The simulated and measured impedance and return loss are shown in Fig. 17(a) and 17(b) respectively. It is observed that measured responses are quite in agreement with the simulated responses for free space and metal surfaces. Small variation is observed from the simulation results on skin surface. The closeness of simulated and measured responses makes the

design suitable for universal item level tagging for near field communication.

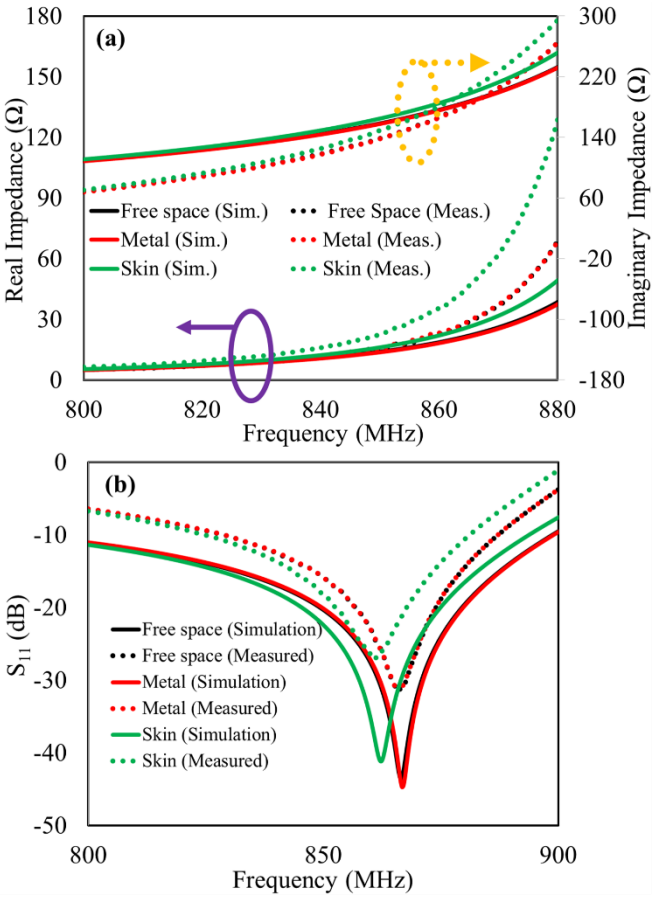

FIGURE 17. Measured and simulated (a) impedance and (b) return losses of proposed antenna.

The reading range and reading rate of the proposed tag are measured using the setup as shown in Fig. 18. The reading range of an RFID tag significantly influences its suitability for various radio frequency (RF) applications. The determination of the maximum reading range of the RFID tag, particularly along the (θ, Φ) direction, is achieved through the application of the Friss transmission equation [2] given in (3).

$$d_{max}(\theta,\varphi) = \frac{c}{4\pi f}\sqrt{\frac{EIRP_R}{P_c}\tau G_{tag}(\theta,\varphi)} \quad (3)$$

Here, $EIRP_R$ is the effective isotropic radiated power (2 W), given by the product of the transmitted power P_t and the antenna gain G_t of the reader, P_c is the minimum threshold RF power required by the chip to turn on and the minimum threshold RF power P_c for the chip used in this design is -20.5 dBm, $G_{tag}(\theta,\varphi)$ is the gain of the tag antenna and 'τ' is the power transmission coefficient between the tag antenna and tag chip impedances given in (4), where $0 \le \tau \le 1$.

$$\tau = 1 - [\Gamma]^2 = \frac{4R_cR_A}{|Z_c+Z_A|^2} \le 1 \quad (4)$$

'Γ' is the reflection coefficient which accounts for the impedance mismatch between the antenna (Z_A) and chip impedance (Z_C) as given in (5).

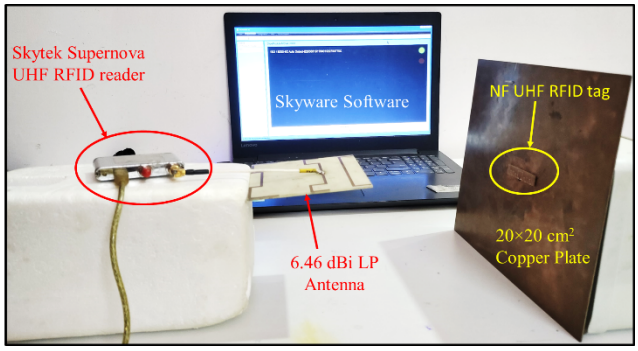

FIGURE 18. Setup for measuring the reading range and reading rate of the proposed tag.

$$\Gamma = \frac{Z_c - Z_A}{Z_c + Z_A} \quad (5)$$

The reading range of the tag is measured by using Skyetek Supernova RFID reader [40] which is connected to a linearly polarized antenna of gain 6.46 dBi. The maximum power is set to 27dBm (0.5Watt) while taking all the measurements. The maximum reading range of the tag was measured, by keeping the tag in motion away from the reader along a straight line up to a point where it can be maximally detectable for point-to-point transmission and reception. The reading range and reading rate of the tag is measured by placing the tag on different materials like metal, plastic, leather, book, glass, on water bottle and skin etc. The tag is also tested inside of the plastic box, leather wallet and, book etc. as shown in Fig. 19.

FIGURE 19. The proposed tag placed on/in different materials.

At first, all the measurement are done by considering the proposed tag with ground and then the measurement are done when the ground is removed from the bottom of the tag. The comparative analyses of the reading range and reading rate are shown in Table V and Table VI respectively. It observed that the tag with ground provides range in a confined region on all applied materials, with a maximum range of 1300 mm when placed in free space. The reading range of the tag can be reduced further by decreasing the size of the antenna, reduction in the thickness of the substrate and use of lossy substrate. Although the tag (without ground) provide good

read rate in some environment as compared with the tag (with ground), but the reading range is not confined in most of the regions as shown in Table V. The designed tag exhibits the minimum reading rate of 212 read per minute as listed in Table VI.

TABLE V Comparative analyses of the measured reading range (mm) of the proposed tag with/without ground plane when placed on different materials.

Material	Read Range (mm) (With Ground) Outside/ Inside	Read Range (mm) (Without Ground) Outside/ Inside
Free space	1300	2000
Plastic	270/265	400/310
Leather wallet	340/320	250/700
Book	230/140	550/310
Glass	190	1150
Water	250	>3000
Skin	350	500
Metal	175	175

TABLE VI. Comparative analyses of the measured read rate (per minute) of the proposed tag with/without ground plane when placed on different materials. (The tag is placed at 10-15 cm from reader antenna)

Material	Reading rate (per minute) (With Ground)	Reading rate (per minute) (Without Ground)
Free space	322	340
Plastic	288	300
Leather wallet	235	260
Book	212	281
Glass	240	245
Water	304	298
Skin	295	290
Metal	270	270

The path gain is also measured to analyse the performance of the tag in near field. The evaluation of the system Path Gain (PG), that is here defined as the following ratio [5] in "(6)"

$$\mathrm{PG} = \frac{P_{Tag\_Threshold}}{P_{Reader\_min}} \qquad (6)$$

$P_{Tag\_Threshold}$ is the threshold power of the chip which is -20.5 dBm, which is taken as reference. P_{Reader_min} is the minimum power applied to the reader, so that it can detect the tag at a particular distance. The measured path gain is shown in -

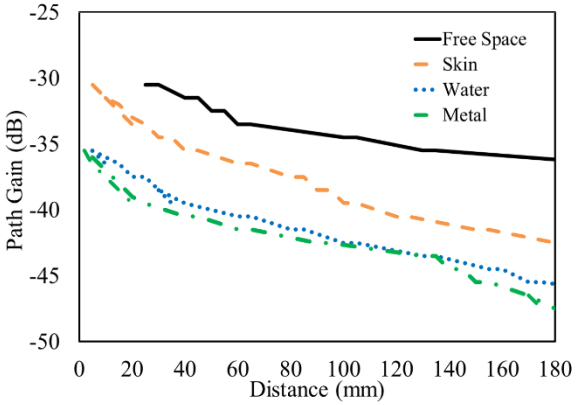

FIGURE 20. Measured path gain (dB) of the tag w.r.t distance for different mountable surfaces.

Fig. 20. It is observed that the antenna is behaving similarly in both near field ($\lambda/2\pi$) as well as in far field. The difference in the path gain for different environment is due to the change in the radiation efficiency and gain of the antenna.

IV. CONCLUSION

A surface-tolerant UHF RFID tag is designed for near-field applications in the ETSI band. The tag's read range and size are constrained by incorporating a ground plane beneath the meandered dipole connected to T-matched loop. The impedance and return loss (S_{11}) of the tag were measured by placing it on different mounting surfaces, including free space, metal, and skin. Additionally, experimental testing of the tag's read range was conducted on various platforms, such as a plastic box, a leather wallet, and inside a book. In all tested configurations, the tag exhibited a confined reading range of less than 350 mm, with a read rate exceeding 212 reads per minute, ensuring reliability in harsh environments. Path gain analysis was performed to evaluate the system's performance in both near-field and far-field scenarios. The grounded tag demonstrated stable performance across all mounting platforms, confirming its platform tolerance. Therefore, the designed tag is suitable for various RFID applications, including item-level tagging, e-payment, ID cards, and e-passports.

REFERENCES

[1] Finkenzeller, RFID Handbook: Fundamentals and Applications in Contactless Smart Cards and Identification, 3rd ed., John Wiley &Sons, 2010.

[2] K. V. S. Rao, P. V. Nikitin and S. F. Lam, "Antenna design for UHF RFID tags: a review and a practical application," in IEEE Transactions on Antennas and Propagation, vol. 53, no. 12, pp. 3870-3876, Dec. 2005, doi: 10.1109/TAP.2005.859919.

[3] S. -Y. Kim, S. -H. Ahn and W. -S. Lee, "Near-Field UHF Quadruple Loop Antenna With Uniform Field Distribution for Item-Level Tagging," in IEEE Antennas and Wireless Propagation Letters, vol. 20, no. 4, pp. 523-527, April 2021, doi: 10.1109/LAWP.2021.3056026.

[4] R. M. Lieshout, L. Grossi, G. Spinelli, S. Helmus, L. Kool, L. Pennings, R. Stap, T. Veugen, B. der Waaij, and C. Borean, *RFID Technologies: Emerging Issues, Challenges and Policy Options*, Tech. Rep. EUR 22770 EN, Institute for Prospective Technological Studies, European Commission, 2007.

[5] F. Fuschini, C. Piersanti, L. Sydanheimo, L. Ukkonen and G. Falciasecca, "Electromagnetic Analyses of Near Field UHF RFID Systems," in *IEEE Transactions on Antennas and Propagation*, vol. 58, no. 5, pp. 1759-1770, May 2010, doi: 10.1109/TAP.2010.2044328.

[6] P. Kolarovszki and J. Vaculík, "Middleware – Software Support in Items Identification by Using the UHF RFID Technology," in *Mobile and Ubiquitous Systems: Computing, Networking, and Services. MobiQuitous 2013*, I. Stojmenovic, Z. Cheng, and S. Guo, Eds. Cham, Switzerland: Springer, 2014, vol. 131, pp. 368-379. doi: 10.1007/978-3-319-11569-6_28.

[7] X. Li and Z. Yang, "Dual-Printed-Dipoles Reader Antenna for UHF Near-Field RFID Applications," in IEEE Antennas and Wireless Propagation Letters, vol. 10, pp. 239-242, 2011, doi: 10.1109/LAWP.2011.2121050.

[8] Y.F. Lin, C.T. Liao, H.M. Chen and Z.D. Jiang. "Compact folded square-loop antenna for reading near-field RFID tags in blood sample

tracking system", in Electronics Letters, vol. 53, pp. 1627-1628, 2017, doi: 10.1049/el.2017.1859.

[9] Y. Zeng, Z. N. Chen, X. Qing and J. -M. Jin, "A Directional, Closely Spaced Zero-Phase-Shift-Line Loop Array for UHF Near-Field RFID Reader Antennas," in IEEE Transactions on Antennas and Propagation, vol. 66, no. 10, pp. 5639-5642, Oct. 2018, doi: 10.1109/TAP.2018.2860619.

[10] Z. Xing, H. Li, C. -Y. -D. Sim, J. Li and Z. Li, "Study of a Multi-Loop Travelling Wave UHF RFID Near-Field Antenna," in IEEE Access, vol. 8, pp. 69829-69837, 2020, doi: 10.1109/ACCESS.2020.2985992.

[11] W. Choi, J.-S. Kim, J.-H. Bae, G. Choi and J.-S. Chae, "Near-field antenna for a radio frequency identification shelf in the UHF band", in IET Microwaves, Antennas & Propagation, Vol. 4,, pp. 1538 – 1542, 2010, doi: 10.1049/iet-map.2009.0203.

[12] M.-G. Jeong, J.-H. Kim, S.-H. Bae, and W.-S. Lee, "Electric-field-coupled contactless ID sensor for cm-level high-precision positioning item level tagging systems", Electronics Letters, Vol. 52 No. 10 pp. 837–838, May 2016, doi: 10.1049/el.2016.0383.

[13] C. R. Medeiros, J. R. Costa and C. A. Fernandes, "RFID Smart Shelf With Confined Detection Volume at UHF," in IEEE Antennas and Wireless Propagation Letters, vol. 7, pp. 773-776, 2008, doi: 10.1109/LAWP.2008.2008672.

[14] C. R. Medeiros, J. R. Costa and C. A. Fernandes, "RFID Reader Antennas for Tag Detection in Self-Confined Volumes at UHF," in IEEE Antennas and Propagation Magazine, vol. 53, no. 2, pp. 39-50, April 2011, doi: 10.1109/MAP.2011.5949323.

[15] Y. Ozawa, Q. Chen, K. Sawaya, M. Oouchida and M. Tokieda, "Design of a Wide Planar Waveguide Antenna for UHF Near-Field RFID Reader With High Reading Rate," in IEEE Journal of Radio Frequency Identification, vol. 5, no. 1, pp. 46-52, March 2021, doi: 10.1109/JRFID.2020.3039016.

[16] G. Lovat, "Near-Field Shielding Effectiveness of 1-D Periodic Planar Screens With 2-D Near-Field Sources," in IEEE Transactions on Electromagnetic Compatibility, vol. 51, no. 3, pp. 708-719, Aug. 2009, doi: 10.1109/TEMC.2009.2022273.

[17] P. Burghignoli, G. Lovat, F. Capolino, D. R. Jackson and D. R. Wilton, "Highly Polarized, Directive Radiation From a Fabry-Pérot Cavity Leaky-Wave Antenna Based on a Metal Strip Grating," in IEEE Transactions on Antennas and Propagation, vol. 58, no. 12, pp. 3873-3883, Dec. 2010, doi: 10.1109/TAP.2010.2078441.

[18] R. Araneo, G. Lovat and S. Celozzi, "Shielding Effectiveness of Periodic Screens Against Finite High-Impedance Near-Field Sources," in IEEE Transactions on Electromagnetic Compatibility, vol. 53, no. 3, pp. 706-716, Aug. 2011, doi: 10.1109/TEMC.2010.2081367.

[19] T. A. Morgado et al., "Spatially Confined UHF RFID Detection With a Metamaterial Grid," in IEEE Transactions on Antennas and Propagation, vol. 62, no. 1, pp. 378-384, Jan. 2014, doi: 10.1109/TAP.2013.2287027.

[20] K. Zannas, H. El Matbouly, Y. Duroc and S. Tedjini, "Self-Tuning RFID Tag: A New Approach for Temperature Sensing," in IEEE Transactions on Microwave Theory and Techniques, vol. 66, no. 12, pp. 5885-5893, Dec. 2018, doi: 10.1109/TMTT.2018.2878568.

[21] C. Miozzi, V. Errico, G. Saggio, E. Gruppioni and G. Marrocco, "UHF RFID-Based EMG for Prosthetic Control: preliminary results," 2019 IEEE International Conference on RFID Technology and Applications (RFID-TA), Pisa, Italy, 2019, pp. 310-313, doi: 10.1109/RFID-TA.2019.8891964.

[22] E. Moradi et al., "Backscattering Neural Tags for Wireless Brain-Machine Interface Systems," in IEEE Transactions on Antennas and Propagation, vol. 63, no. 2, pp. 719-726, Feb. 2015, doi: 10.1109/TAP.2014.2384038.

[23] M. W. A. Khan, L. Sydänheimo, L. Ukkonen and T. Björninen, "Inductively Powered Pressure Sensing System Integrating a Far-Field Data Transmitter for Monitoring of Intracranial Pressure," in IEEE Sensors Journal, vol. 17, no. 7, pp. 2191-2197, 1 April1, 2017, doi: 10.1109/JSEN.2017.2661324.

[24] F. Naccarata, G. M. Bianco and G. Marrocco, "Sensing Performance of Multi-Channel RFID-Based Finger Augmentation Devices for Tactile Internet," in *IEEE Journal of Radio Frequency Identification*, vol. 6, pp. 209-217, 2022, doi: 10.1109/JRFID.2022.3178348.

[25] G. M. Bianco, S. Amendola and G. Marrocco, "Near-Field Constrained Design for Self-Tuning UHF-RFID Antennas," in IEEE Transactions on Antennas and Propagation, vol. 68, no. 10, pp. 6906-6911, Oct. 2020, doi: 10.1109/TAP.2020.2995315.

[26] Sharif, A., Yan, Y., Ouyang, J., Chattha, H.T.; Arshad, K., Assaleh, K., Alotabi, A.A., Althobaiti, T., Ramzan, N., Abbasi, Q.H., "Uniform Magnetic Field Characteristics Based UHF RFID Tag for Internet of Things Applications", in Electronics, vol. 10, pp. 1603, 2021, doi: 10.3390/electronics10131603.

[27] Sajal, Sayeed & Braaten, Benjamin & Marinov, Val & Swenson, Orven & Atanasov, Yuriy. "A low-cost compact antenna design on a paper substrate for near-field passive UHF RFID tags", in Microwave and Optical Technology Letters. Vol. 59. Pp. 1052-1056, 2017, doi: 10.1002/mop.30460.

[28] K. Jaakkola and P. Koivu, "Low-Cost and Low-Profile Near Field UHF RFID Transponder for Tagging Batteries and Other Metal Objects," in IEEE Transactions on Antennas and Propagation, vol. 63, no. 2, pp. 692-702, Feb. 2015, doi: 10.1109/TAP.2014.2378260.

[29] X. -B. Sun, J. Xie and M. -Y. Cao, "RFID Tag Antenna Design Based on an Improved Coupling Source Shape," in IEEE Antennas and Wireless Propagation Letters, vol. 12, pp. 532-534, 2013, doi: 10.1109/LAWP.2013.2255856.

[30] G. Zamora, S. Zuffanelli, F. Paredes, F. Martı´n and J. Bonache, "Design and Synthesis Methodology for UHF-RFID Tags Based on the T-Match Network," in IEEE Transactions on Microwave Theory and Techniques, vol. 61, no. 12, pp. 4090-4098, Dec. 2013, doi: 10.1109/TMTT.2013.2287856.

[31] P. V. Nikitin, K. V. S. Rao and S. Lazar, "An Overview of Near Field UHF RFID," 2007 IEEE International Conference on RFID, Grapevine, TX, USA, 2007, pp. 167-174, doi: 10.1109/RFID.2007.346165.

[32] Choudhary, Abhishek & Gopal, Krishan & Sood, Deepak & Tripathi, Chandra Charu,." Development of compact inductive coupled meander line RFID tag for near-field applications", in International Journal of Microwave and Wireless Technologies , Vol. 9, , May 2017 , pp. 757 – 764, doi: 10.1017/S1759078716000751.

[33] K. Carver and J. Mink, "Microstrip antenna technology," in *IEEE Transactions on Antennas and Propagation*, vol. 29, no. 1, pp. 2-24, January 1981, doi: 10.1109/TAP.1981.1142523.

[34] T. Björninen, L. Sydänheimo, L. Ukkonen and Y. Rahmat-Samii, "Advances in antenna designs for UHF RFID tags mountable on conductive items," in IEEE Antennas and Propagation Magazine, vol. 56, no. 1, pp. 79-103, Feb. 2014, doi: 10.1109/MAP.2014.6821761.

[35] Higgs 4 IC Datasheet, An EPCglobal Complaint Class-1 Gen-2 ISO/ IEC 18000-6C UHF RFID Integrated Circuit, Alien Technology, Available: http://www.Alientechnology.com.

[36] M. M. Rahman and A. K. Sarkar, "A method for calculating the resonant frequency of meander line dipole antenna by using antenna's geometrical parameters," 2017 6th International Conference on Informatics, Electronics and Vision & 2017 7th International Symposium in Computational Medical and Health Technology (ICIEV-ISCMHT), Himeji, Japan, 2017, pp. 1-6, doi: 10.1109/ICIEV.2017.8338589.

[37] T. Endo, Y. Sunahara, S. Satoh and T. Katagi, "Resonant frequency and radiation efficiency of meander line antennas", Electronics and Communications in Japan (Part II: Electronics), vol. 83, pp. 52-58, 2000, doi: 10.1002/(SICI)1520-6432(200001)83:1<52::AID-ECJB7>3.0.CO;2-7

[38] X. Qing, C. K. Goh and Z. N. Chen, "Impedance Characterization of RFID Tag Antennas and Application in Tag Co-Design," in IEEE Transactions on Microwave Theory and Techniques, vol. 57, no. 5, pp. 1268-1274, May 2009, doi: 10.1109/TMTT.2009.2017288.

[39] S. Amendola, S. Milici and G. Marrocco, "Performance of Epidermal RFID Dual-loop Tag and On-Skin Retuning," in *IEEE Transactions on Antennas and Propagation*, vol. 63, no. 8, pp. 3672-3680, Aug. 2015, doi: 10.1109/TAP.2015.2441211.

[40] UHF RFID reader Skyetek Supernova, Available: www.jadaktech.com.